Crystal-orientation effects on the piezoelectric field and electronic properties of strained wurtzite semiconductors

Seoung-Hwan Park* and Shun-Lien Chuang†
Department of Electrical and Computer Engineering, University of Illinois at Urbana-Champaign, 1406 West Green Street, Urbana, Illinois 61801

(Received 1 June 1998; revised manuscript received 29 October 1998)

Crystal orientation effects on the piezoelectric field and electronic properties of strained GaN bulk semiconductors are investigated. Analytical expressions for the band gap, wave function, and momentum matrix element of strained wurtzite GaN using a recently derived block-diagonalized Hamiltonian are shown. We find that the energy separation between the top two valence bands increases with the angle θ between the growth (z') direction and the c axis. This results in a significant reduction of the effective mass of the top valence band along the transverse (k_x') direction with increasing angle for both compressively and tensilely strained GaN crystals. Similar results are observed in the valence-band dispersion relations for the quantum-well (QW) structure. The dispersion curves for the QW structure also show a lifting of the Kramers degeneracy due to the piezoelectric field, which causes an asymmetry in the potential. We find that the optical matrix element of the TE polarization between the conduction (C) and heavy hole (HH) bands of the compressively strained GaN for a growth direction with $\theta \geqslant 30°$ is about twice as large as that of the (0001) orientation ($\theta = 0°$). The piezoelectric polarizations of the compressive and tensile strains are plotted as a function of the growth direction. The crystal orientation at which a maximum polarization occurs is shown as a function of strain. In particular, the GaN crystal along the $(10\bar{1}0)$ growth direction ($\theta = 90°$) shows zero normal piezoelectric polarization (P_z') for the compressive and tensile strains. These results show that crystal orientation dependence of the piezoelectric field and strain significantly affect the electronic transport properties as well as optical interband absorption properties. [S0163-1829(99)03008-8]

I. INTRODUCTION

Wide-band-gap semiconductors including GaN, AlN, and InN, and their ternary compounds, have great potential for applications in high-power optoelectronic devices in the blue and ultraviolet regions. Blue-green light-emitting diodes based on wurtzite $In_xGa_{1-x}N/Al_yGa_{1-y}N$ quantum-well (QW) structures have been realized recently.[1,2] Room-temperature continuous-wave operation of strained $In_xGa_{1-x}N/Al_yGa_{1-y}N$ multiple quantum-well laser diodes with a lifetime of many thousand hours have been demonstrated.[3]

To understand wurtzite semiconductor properties, the Hamiltonian near the band edges is important because the band structure near the direct band edges determines most of the fundamental electronic and optical properties. The Hamiltonian near the band edge of the wurtzite semiconductor has been derived using the invariant method based on the symmetry properties of the wurtzite structure,[4–6] and many of the band-structure parameters have been treated empirically. On the other hand, the $\mathbf{k}\cdot\mathbf{p}$ method has also been used to derive the Hamiltonian, and a block diagonalization has been shown.[7,8] The $\mathbf{k}\cdot\mathbf{p}$ method is attractive since the Hamiltonian has explicit definitions of the band-structure and interband optical momentum matrix elements.

In zinc-blende crystals, a biaxial compressive strain in a QW structure reduces the in-plane effective mass of the top heavy-hole band and the threshold current of a semiconductor laser.[9] On the other hand, the hole effective mass of GaN is significantly larger than that of conventional zinc-blende crystals used in semiconductor lasers, such as GaAs and InP. It has been shown that the introduction of biaxial strain into the (0001) plane of a wurtzite GaN-based crystal does not effectively reduce the effective masses in the transverse direction,[10–12] unlike in other III-V semiconductors. This is due to the fact that, for a wurtzite layer grown along the (0001) orientation, the strain shifts both the heavy-hole and light-hole bands by almost the same amount, and the in-plane effective masses remain almost the same as those in the unstrained case.[8,13] Also, GaN heterostructures with a wurtzite crystal structure pseudomorphically grown in the (0001) orientation have a large strain-induced piezoelectric field.[14–17] It was shown that the optical gain in QW lasers is largely reduced due to the piezoelectric field at relatively low carrier densities.[18,19] On the other hand, electrical and optical properties in wurtzite[14,15,20] and zinc-blende[21,22] semiconductors can be affected by their crystal orientation. Therefore, the crystal orientation will significantly modify the strain-induced band structures. Despite their importance, many fundamental crystal orientation effects on wurtzite semiconductor properties are still not well understood.

In this paper, we investigate crystal orientation effects on the piezoelectric field and electronic properties of strained GaN bulk semiconductors, and present analytical solutions and numerical results for the band gaps, wave functions, and optical matrix elements at the band edges as a function of the crystal orientation. The effective mass near the band edge and the piezoelectric field are also investigated as functions of the crystal orientation. The analytical expressions will be useful for understanding the crystal orientation effects on the

physical properties of GaN. In addition to analytical expressions, we consider the quantum-well structure to show the piezoelectric field effect on the valence energy dispersion relation, which shows a lifting of the Kramers degeneracy.

In Sec. II, we derive analytical expressions for the strain components, the piezoelectric field, eigenenergies, band gaps, wave functions, and optical matrix elements for an arbitrary crystal orientation of the strained wurtzite GaN. The 6×6 Hamiltonian for the valence bands at the band edge is block diagonalized into two 3×3 Hamiltonians, which have analytical solutions for eigenvectors and eigenenergies. The quantum-well structure with the piezoelectric field is also considered. In Sec. III, numerical results for crystal orientation effects on the piezoelectric field and electronic properties of wurtzite GaN semiconductor are shown. We then conclude in Sec. IV.

II. THEORY

A. The Hamiltonian and strain tensors

The Hamiltonian for the valence-band structure has been derived by the $\mathbf{k}\cdot\mathbf{p}$ method.[8] The full Hamiltonian for (0001)-oriented wurtzite crystal can be written as

$$H(\mathbf{k},\boldsymbol{\epsilon})=\begin{pmatrix} F & -K^* & -H^* & 0 & 0 & 0 \\ -K & G & H & 0 & 0 & \Delta \\ -H & H^* & \lambda & 0 & \Delta & 0 \\ 0 & 0 & 0 & F & -K & H \\ 0 & 0 & \Delta & -K^* & G & -H^* \\ 0 & \Delta & 0 & H^* & -H & \lambda \end{pmatrix} \begin{matrix} |U_1\rangle \\ |U_2\rangle \\ |U_3\rangle \\ |U_4\rangle \\ |U_5\rangle \\ |U_6\rangle, \end{matrix} \tag{1}$$

where

$$\begin{aligned} F&=\Delta_1+\Delta_2+\lambda+\theta, \\ G&=\Delta_1-\Delta_2+\lambda+\theta, \\ \lambda&=\frac{\hbar^2}{2m_o}[A_1k_z^2+A_2(k_x^2+k_y^2)]+\lambda_\epsilon, \\ \theta&=\frac{\hbar^2}{2m_o}[A_3k_z^2+A_4(k_x^2+k_y^2)]+\theta_\epsilon, \\ K&=\frac{\hbar^2}{2m_o}A_5(k_x+ik_y)^2+D_5\epsilon_+, \\ H&=\frac{\hbar^2}{2m_o}A_6(k_x+ik_y)k_z+D_6\epsilon_{z+}, \\ \lambda_\epsilon&=D_1\epsilon_{zz}+D_2(\epsilon_{xx}+\epsilon_{yy}), \\ \theta_\epsilon&=D_3\epsilon_{zz}+D_4(\epsilon_{xx}+\epsilon_{yy}), \\ \epsilon_+&=\epsilon_{xx}-\epsilon_{yy}+2i\epsilon_{xy}, \\ \epsilon_{z+}&=\epsilon_{xz}+i\epsilon_{yz}, \\ \Delta&=\sqrt{2}\Delta_3. \end{aligned} \tag{2}$$

Here the A_i's are the valence-band effective-mass parameters, which are similar to the Luttinger parameters in a zinc-blende crystal; the D_i's are the deformation potentials for wurtzite crystals; k_i is the wave vector; ϵ_{ij} is the strain tensor; Δ_1 is the crystal-field-split energy; and Δ_2 and Δ_3 account for spin-orbit interactions. The bases for the Hamiltonian are defined as[8]

$$\begin{aligned} |U_1\rangle&=-\frac{1}{\sqrt{2}}|(X+iY)\uparrow\rangle, \\ |U_2\rangle&=\frac{1}{\sqrt{2}}|(X-iY)\uparrow\rangle, \\ |U_3\rangle&=|Z\uparrow\rangle, \\ |U_4\rangle&=\frac{1}{\sqrt{2}}|(X-iY)\downarrow\rangle, \\ |U_5\rangle&=-\frac{1}{\sqrt{2}}|(X+iY)\downarrow\rangle, \\ |U_6\rangle&=|Z\downarrow\rangle. \end{aligned} \tag{3}$$

The Hamiltonian for an arbitrary crystal orientation can be obtained using a rotation matrix

$$U=\begin{pmatrix} \cos\theta\cos\phi & \cos\theta\sin\phi & -\sin\theta \\ -\sin\phi & \cos\phi & 0 \\ \sin\theta\cos\phi & \sin\theta\sin\phi & \cos\theta \end{pmatrix}. \tag{4}$$

The rotation of the Euler angles θ and ϕ transforms physical quantities from (x,y,z) coordinates to (x',y',z') coordinates. We consider only the θ dependence of physical quantities in the following due to the hexagonal symmetry.[14] The z axis corresponds to the c axis [0001], and the growth axis (de-

fined as the z' axis) is normal to the QW plane (*hkil*), as shown in Fig. 1. The relations between the coordinate systems for vectors and tensors are expressed as[21,23]

$$k_i' = U_{i\alpha} k_\alpha ,$$

$$\epsilon_{ij}' = U_{i\alpha} U_{j\beta} \epsilon_{\alpha\beta} , \tag{5}$$

$$C_{ijkl}' = U_{i\alpha} U_{j\beta} U_{i\gamma} U_{j\delta} C_{\alpha\beta\gamma\delta} ,$$

where summations over repeated indices are indicated.

The strain coefficients in the (x,y,z) coordinates for a general crystal orientation are determined from the condition that the layer is grown pseudomorphically, and these strain coefficients should minimize the strain energy of the layer simultaneously.[14,24] We define the unit vectors $\hat{\mathbf{x}}'$, $\hat{\mathbf{y}}'$, and $\hat{\mathbf{z}}'$ along the $\mathbf{x}'$, $\mathbf{y}'$, and $\mathbf{z}'$ axes, and they are related to unit vectors $\hat{\mathbf{x}}$, $\hat{\mathbf{y}}$, and $\hat{\mathbf{z}}$ along the $\mathbf{x}$, $\mathbf{y}$, and $\mathbf{z}$ axes through the rotation matrix (4). The hexagonal primitive translational vectors are

$$\boldsymbol{\alpha}_i = a_i \hat{\mathbf{x}},$$

$$\boldsymbol{\beta}_i = \frac{a_i}{2}\hat{\mathbf{x}} + \frac{\sqrt{3} a_i}{2}\hat{\mathbf{y}}, \tag{6}$$

$$\boldsymbol{\gamma}_i = c_i \hat{\mathbf{z}},$$

where a is the lattice constant and i labels the epilayer (e) and the substrate (s). When the crystal is translated, the primitive translational vectors become[9]

$$\boldsymbol{\alpha}_i'' = a_i \hat{\mathbf{x}}'',$$

$$\boldsymbol{\beta}_i'' = \frac{a_i}{2}\hat{\mathbf{x}}'' + \frac{\sqrt{3} a_i}{2}\hat{\mathbf{y}}'', \tag{7}$$

$$\boldsymbol{\gamma}_i'' = c_i \hat{\mathbf{z}}'',$$

where

$$\hat{\mathbf{x}}'' = (1+\epsilon_{xx})\hat{\mathbf{x}} + \epsilon_{xy}\hat{\mathbf{y}} + \epsilon_{xz}\hat{\mathbf{z}},$$

$$\hat{\mathbf{y}}'' = \epsilon_{yx}\hat{\mathbf{x}} + (1+\epsilon_{yy})\hat{\mathbf{y}} + \epsilon_{yz}\hat{\mathbf{z}}, \tag{8}$$

$$\hat{\mathbf{z}}'' = \epsilon_{zx}\hat{\mathbf{x}} + \epsilon_{zy}\hat{\mathbf{y}} + (1+\epsilon_{zz})\hat{\mathbf{z}}.$$

When the first atomic layers are deposited on the substrate, these layers will be strained to match the substrate, and a pseudomorphic (or coherent) interface will be formed. Thus the condition for a pseudomorphic interface means that the

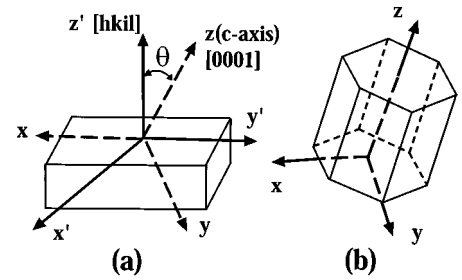

FIG. 1. (a) Configuration of the coordinate systems (x',y',z') in (*hkil*)-oriented crystals. The growth axis, or z' axis, is normal to the substrate surface (*hkil*), and the coordinate system (x,y,z) denotes the primary crystallographic axes. (b) The coordinate system in a wurtzite primitive cell. The angle θ is defined as the angle between the growth direction $\hat{z}'$ and the c axis; $\theta = 0°$ corresponds to the $\hat{z}' = (0001)$ growth direction and $\theta = 90°$ corresponds to the $\hat{z}' = (10\bar{1}0)$ growth direction.

projections of the strain-distorted primitive translational vectors of the epilayer and the substrate on the growth plane should be equal:

$$\begin{aligned} \alpha_e'' \cdot \hat{\mathbf{x}}' &= \alpha_s'' \cdot \hat{\mathbf{x}}', \\ \alpha_e'' \cdot \hat{\mathbf{y}}' &= \alpha_s'' \cdot \hat{\mathbf{y}}', \end{aligned} \tag{9}$$

with analogous conditions on β'' and γ''. Here we assume that the substrate is unstrained. Then, the constraints (9) yield the following relations for the strain tensors:

$$\begin{aligned} \epsilon_{xx} &= \epsilon_{xx}^{(0)} + \epsilon_{xz}\frac{\sin\theta}{\cos\theta}, \\ \epsilon_{yy} &= \epsilon_{xx}^{(0)}, \\ \epsilon_{zz} &= \epsilon_{xz}\frac{\cos\theta}{\sin\theta} + \epsilon_{zz}^{(0)}, \\ \epsilon_{xy} &= \epsilon_{yz} = 0, \end{aligned} \tag{10}$$

where $\epsilon_{xx}^{(0)} = (a_s - a_e)/a_e$ and $\epsilon_{zz}^{(0)} = (c_s - c_e)/c_e$. Under the engineering notation described further in Sec. II D, the strain energy density is given by

$$\begin{aligned} W = \tfrac{1}{2}[& C_{11}\epsilon_{xx}^2 + C_{11}\epsilon_{yy}^2 + C_{33}\epsilon_{zz}^2 + 2C_{12}\epsilon_{xx}\epsilon_{yy} + 2C_{13} \\ & \times(\epsilon_{xx}\epsilon_{zz} + \epsilon_{yy}\epsilon_{zz}) + 4C_{44}\epsilon_{xz}^2]. \end{aligned} \tag{11}$$

Using the above relations, the strain energy can be expressed through only one strain component ϵ_{xz}, which can be found by minimizing the strain energy with respect to the variable ϵ_{xz}. This procedure gives the following expression for ϵ_{xz}.

$$\epsilon_{xz} = -\frac{[(c_{11}+c_{12}+c_{13}\epsilon_{zz}^{(0)}/\epsilon_{xx}^{(0)})\sin^2\theta + (2c_{13}+c_{33}\epsilon_{zz}^{(0)}/\epsilon_{xx}^{(0)})\cos^2\theta]\epsilon_{xx}^{(0)}\cos\theta\sin\theta}{c_{11}\sin^4\theta + 2(c_{13}+2c_{44})\sin^2\theta\cos^2\theta + c_{33}\cos^4\theta}. \tag{12}$$

Hence we obtain a 6×6 Hamiltonian in the (x',y',z') coordinates by substituting the transformation relation for the vector k in Eq. (5) and the strain coefficients for a general crystal orientation into the Hamiltonian (1) for the (0001) orientation.

B. Conduction-band edge of bulk wurtzite semiconductors

The conduction bands of a bulk wurtzite crystal can be characterized by a parabolic band model, and the effective-mass Hamiltonian can be written as[8]

$$H(\mathbf{k})=\frac{\hbar^2}{2}\left(\frac{k_x^2+k_y^2}{m_e^t}+\frac{k_z^2}{m_e^z}\right)+E_c^0+P_{c\epsilon}, \tag{13}$$

where the band-edge energy is given by

$$E_c^0=\Delta_1+\Delta_2+E_g+P_{c\epsilon}, \tag{14}$$

which includes a hydrostatic energy shift

$$P_{c\epsilon}=a_{cz}\epsilon_{zz}+a_{ct}(\epsilon_{xx}+\epsilon_{yy}), \tag{15}$$

where a_{cz} and a_{ct} are the conduction-band deformation potentials along the c axis and perpendicular to the c axis. We take $a_{cz}=a_{ct}$ for simplicity, and assume a value of -4.08 eV from a recent fit[8,13] to the available experimental data. The conduction-band wave function of a bulk wurtzite semiconductor is of the form

$$\Psi^{c\eta}(\mathbf{r},\mathbf{k})=\frac{1}{\sqrt{V}}e^{i\mathbf{k}\cdot\mathbf{r}}|S\eta\rangle, \tag{16}$$

where $\eta=\uparrow$ or $\downarrow$, and S is a spherically symmetric wave function.

C. Valence-band edges of bulk wurtzite semiconductors

At the band edges, $k_x'=k_y'=k_z'=0$, the Hamiltonian in the (x',y',z') coordinates can be simplified:

$$H'(\mathbf{k}'=0,\boldsymbol{\epsilon})=\begin{pmatrix} F' & -K'^* & -H'^* & 0 & 0 & 0\\ -K' & G' & H' & 0 & 0 & \Delta\\ -H' & H'^* & \lambda' & 0 & \Delta & 0\\ 0 & 0 & 0 & F' & -K' & H'\\ 0 & 0 & \Delta & -K'^* & G' & -H'^*\\ 0 & \Delta & 0 & H'^* & -H' & \lambda' \end{pmatrix}\begin{matrix}|U_1\rangle'\\|U_2\rangle'\\|U_3\rangle'\\|U_4\rangle'\\|U_5\rangle'\\|U_6\rangle',\end{matrix} \tag{17}$$

where

$$\begin{aligned} F'&=\Delta_1+\Delta_2+\lambda_\epsilon'+\theta_\epsilon',\\ G'&=\Delta_1-\Delta_2+\lambda_\epsilon'+\theta_\epsilon',\\ K'&=D_5(\epsilon_{xx}-\epsilon_{yy}),\\ H'&=D_6\epsilon_{xz},\\ \lambda_\epsilon'&=D_1\epsilon_{zz}+D_2(\epsilon_{xx}+\epsilon_{yy}),\\ \theta_\epsilon'&=D_3\epsilon_{zz}+D_4(\epsilon_{xx}+\epsilon_{yy}),\\ \Delta&=\sqrt{2}\Delta_3, \end{aligned} \tag{18}$$

and the strain coefficients ϵ_{ij} for a general crystal orientation θ are given by Eqs. (10) and (12) in Sec. II A. Note that K' and H' are not zero because $\epsilon_{xx}\neq\epsilon_{yy}$ and $\epsilon_{xz}\neq0$ in the general coordinates. Also, all elements are constant. This Hamiltonian can be block diagonalized following a similar procedure to that used before.[8] The transformation matrix is defined as

$$T=\begin{pmatrix} \alpha^* & 0 & 0 & \alpha & 0 & 0\\ 0 & \beta & 0 & 0 & \beta^* & 0\\ 0 & 0 & \beta^* & 0 & 0 & \beta\\ \alpha^* & 0 & 0 & -\alpha & 0 & 0\\ 0 & \beta & 0 & 0 & -\beta^* & 0\\ 0 & 0 & -\beta^* & 0 & 0 & \beta \end{pmatrix}, \tag{19}$$

where

$$\alpha=\frac{1}{\sqrt{2}}e^{i(3\pi/4)},\quad \beta=\frac{1}{\sqrt{2}}e^{i(\pi/4)} \tag{20}$$

These expressions are similar to those in Ref. 8, except that $k_x'=k_y'=k_z'=0$, and K' and H' contain nonzero strain components. The block-diagonalized Hamiltonian $H''=T^*H'T^t$ is given by

$$H''=\begin{pmatrix} H'^U & 0\\ 0 & H'^L \end{pmatrix}, \tag{21}$$

where the upper 3×3 Hamiltonian is

$$H'^U=\begin{pmatrix} F' & K' & -iH'\\ K' & G' & \Delta-iH'\\ iH' & \Delta+iH' & \lambda' \end{pmatrix} \tag{22}$$

and the lower 3×3 Hamiltonian is

$$H'^L=\begin{pmatrix} F' & K' & iH'\\ K' & G' & \Delta+iH'\\ -iH' & \Delta-iH' & \lambda' \end{pmatrix}. \tag{23}$$

The lower Hamiltonian is the complex conjugate of the upper Hamiltonian. Therefore, they have exactly the same eigenvalues since the eigenenergies are real. However, for the QW structure, there will be a lifting of the Kramers degeneracy[25,26] in the in-plane dispersion relations because of the piezoelectric field, which will be discussed in Sec.

II E. The wave functions of the lower Hamiltonian are the complex conjugates of the corresponding wave functions of the upper Hamiltonian. The eigenequation for the valence band energy E' at the band edge is given by

$$\begin{pmatrix} F'-E' & K' & -iH' \\ K' & G'-E' & \Delta-iH' \\ iH' & \Delta+iH' & \lambda'-E' \end{pmatrix} \begin{pmatrix} g_1' \\ g_2' \\ g_3' \end{pmatrix} = 0. \tag{24}$$

The eigenequation is a third-order polynomial equation, which can always be solved analytically. These three analytical solutions can be expressed as[13,27]

$$\begin{aligned} E_1' &= 2(S_1+S_2)-\frac{C_2}{3}, \\ E_2' &= -\frac{1}{2}(S_1+S_2)-\frac{C_2}{3}+i\frac{\sqrt{3}}{2}(S_1-S_2), \\ E_3' &= -\frac{1}{2}(S_1+S_2)-\frac{C_2}{3}-i\frac{\sqrt{3}}{2}(S_1-S_2), \end{aligned} \tag{25}$$

where

$$\begin{aligned} q &= \frac{1}{3}C_1-\frac{1}{9}C_2^2, \\ r &= \frac{1}{6}(C_1C_2-3C_0)-\frac{C_2^3}{27}, \\ S_1 &= [r+\sqrt{q^3+r^2}]^{1/3}, \\ S_2 &= [r-\sqrt{q^3+r^2}]^{1/3}, \end{aligned} \tag{26}$$

and

$$\begin{aligned} C_0 &= -(F'G'\lambda'+2K'H'^2-H'^2G' \\ &\quad -K'^2\lambda'-F'\Delta^2-F'H'^2), \\ C_1 &= G'\lambda'+F'\lambda'+F'G'-\Delta^2-2H'^2-K'^2, \\ C_2 &= -(G'+F'+\lambda). \end{aligned} \tag{27}$$

The envelope functions corresponding to the three eigenvalues are determined by

$$\begin{pmatrix} g_1' \\ g_2' \\ g_3' \end{pmatrix} = \frac{1}{D}\begin{pmatrix} D_1 \\ D_2 \\ D_3 \end{pmatrix}, \tag{28}$$

where

$$\begin{aligned} D_1 &= iH'(G'-E')+(\Delta-iH')K', \\ D_2 &= iH'K'(F'-E')(\Delta-iH'), \\ D_3 &= (F'-E')(G'-E')-K'^2, \end{aligned} \tag{29}$$

and

$$D = \sqrt{|D_1|^2+|D_2|^2+|D_3|^2}. \tag{30}$$

The complete Bloch wave functions for the valence band are given by

$$\Psi'^{v}(\mathbf{r}',\mathbf{k}'=0) = \frac{1}{\sqrt{V}}e^{i\mathbf{k}'\cdot\mathbf{r}'}\sum_{i=1}^{3} g_i'(\mathbf{k}')|i\rangle', \tag{31}$$

where

$$\begin{aligned} |1\rangle' &= \alpha^*|U_1\rangle'+\alpha|U_4\rangle', \\ |2\rangle' &= \beta|U_2\rangle'+\beta^*|U_5\rangle', \\ |3\rangle' &= \beta^*|U_3\rangle'+\beta|U_6\rangle', \end{aligned} \tag{32}$$

and we can obtain similar expressions for the lower Hamiltonian (23).

D. Polarization-dependent interband optical-matrix elements

The optical momentum matrix elements in the (x',y',z') coordinates are given by

$$|\hat{\mathbf{e}}'\cdot\mathbf{M}'^{\eta}|^2 = |\langle\Psi'^{c\eta}|\hat{\mathbf{e}}'\cdot\mathbf{p}'|\Psi'^{v}\rangle|^2. \tag{33}$$

Using the expressions for the band-edge wave functions of the conduction and valence bands given in Eqs. (16), (28), and (31), we obtain the following polarization-dependent interband momentum-matrix elements: the TE polarizations ($\hat{\mathbf{e}}'=\hat{\mathbf{x}}'$ or $\hat{\mathbf{y}}'$)

$$|M_{x'}'^{,\eta}|^2 = \left|-\frac{1}{\sqrt{2}}g_1'\alpha^*\cos\theta\langle S|p_x|X\rangle+\frac{1}{\sqrt{2}}g_2'\beta\cos\theta\langle S|p_x|X\rangle-g_3'\beta^*\sin\theta\langle S|p_z|Z\rangle\right|^2 \quad \text{for } \sigma=U \tag{34}$$

$$= \left|-\frac{1}{\sqrt{2}}g_4'\alpha^*\cos\theta\langle S|p_x|X\rangle+\frac{1}{\sqrt{2}}g_5'\beta\cos\theta\langle S|p_x|X\rangle+g_6'\beta^*\sin\theta\langle S|p_z|Z\rangle\right|^2 \quad \text{for } \sigma=L; \tag{35}$$

and the TM polarization ($\hat{\mathbf{e}}'=\hat{\mathbf{z}}'$)

$$|M_{z'}'^{,\eta}|^2 = \left|-\frac{1}{\sqrt{2}}g_1'\alpha^*\sin\theta\langle S|p_x|X\rangle+\frac{1}{\sqrt{2}}g_2'\beta\sin\theta\langle S|p_x|X\rangle+g_3'\beta^*\cos\theta\langle S|p_z|Z\rangle\right|^2 \quad \text{for } \sigma=U \tag{36}$$

$$= \left| -\frac{1}{\sqrt{2}} g_4' \alpha^* \sin\theta \langle S|p_x|X\rangle + \frac{1}{\sqrt{2}} g_5' \beta \sin\theta \langle S|p_x|X\rangle - g_6' \beta^* \cos\theta \langle S|p_z|Z\rangle \right|^2 \quad \text{for } \sigma = L. \tag{37}$$

The above analytical results include the crystal orientation dependence, and the band-edge matrix elements are derived[8] using the same procedure as in the derivation of Kane's parameters (P_1 and P_2):

$$\begin{aligned} \langle S|p_x|X\rangle &= \frac{m_0}{\hbar} P_2, \\ \langle S|p_z|Z\rangle &= \frac{m_0}{\hbar} P_1, \\ P_1^2 &= \frac{\hbar^2}{2m_o}\left(\frac{m_o}{m_e^z} - 1\right)\frac{(E_g+\Delta_1+\Delta_2)(E_g+2\Delta_2)-2\Delta_3^2}{E_g+2\Delta_2}, \\ P_2^2 &= \frac{\hbar^2}{2m_o}\left(\frac{m_o}{m_e^t} - 1\right)\frac{E_g[(E_g+\Delta_1+\Delta_2)(E_g+2\Delta_2)-2\Delta_3^2]}{(E_g+\Delta_1+\Delta_2)(E_g+\Delta_2)-\Delta_3^2}. \end{aligned} \tag{38}$$

Substituting $E' = E_1'$, E_2', and E_3', we can obtain moment matrix element for the interband optical transitions between the conduction (C) band and the heavy hole, light hole, and crystal-field split-off hole bands, respectively.

E. Piezoelectric field and valence-band structure of a quantum well

If a stress τ_{jk} is applied to GaN crystals, there is an induced piezoelectric polarization with a magnitude proportional to the applied stress τ_{jk}:

$$P_i = d_{ijk}\tau_{jk}, \tag{39}$$

where d_{ijk} are the piezoelectric moduli or piezoelectric tensor elements. The stress τ_{ij} is related to the strain by

$$\tau_{ij} = c_{ijkl}\epsilon_{kl}, \tag{40}$$

where c_{ijkl} are the stiffness constants of the wurtzite GaN crystal. Here it is convenient to replace the tensor notation by the the engineering notation for d_{ijk} and c_{ijkl} using their symmetry properties.[23] That is, the second and third subscripts in d_{ijk} and the first two and last two subscripts in c_{ijkl} are replaced by a single subscript running from 1 to 6 as follows:

tensor notation	11	22	33	23,32	31,13	12,21,
matrix notation	1	2	3	4	5	6.

Then the piezoelectric polarization in the (x,y,z) coordinates for a general crystal orientation is given by

$$\begin{pmatrix} P_x \\ P_y \\ P_z \end{pmatrix} = \begin{pmatrix} 0 & 0 & 0 & 0 & d_{15} & 0 \\ 0 & 0 & 0 & d_{15} & 0 & 0 \\ d_{31} & d_{31} & d_{33} & 0 & 0 & 0 \end{pmatrix} \begin{pmatrix} c_{11} & c_{12} & c_{13} & 0 & 0 & 0 \\ c_{12} & c_{11} & c_{13} & 0 & 0 & 0 \\ c_{13} & c_{13} & c_{33} & 0 & 0 & 0 \\ 0 & 0 & 0 & c_{44} & 0 & 0 \\ 0 & 0 & 0 & 0 & c_{44} & 0 \\ 0 & 0 & 0 & 0 & 0 & c_{66} \end{pmatrix} \begin{pmatrix} \epsilon_{xx} \\ \epsilon_{yy} \\ \epsilon_{zz} \\ 0 \\ 2\epsilon_{xz} \\ 0 \end{pmatrix}, \tag{41}$$

where the strain coefficients in the (x,y,z) coordinates for a general crystal orientation are given in Sec. I. We then obtain the polarization components along x, y, and z axes:

$$\begin{aligned} P_x &= 2d_{15}c_{44}\epsilon_{xz}, \\ P_y &= 0, \\ P_z &= [d_{31}(c_{11}+c_{12})+d_{33}c_{13}](\epsilon_{xx}+\epsilon_{yy}) \\ &\quad + [2d_{31}c_{13}+d_{33}c_{33}]\epsilon_{zz}. \end{aligned} \tag{42}$$

The normal polarization with respect to the growth plane (along the growth direction) can be obtained by taking the scalar product between the polarization vector $\mathbf{P}$ in the (x,y,z) coordinates and the unit vector $\hat{z}'$ shown in Fig. 1:

$$P_z' = \mathbf{P}\cdot\hat{\mathbf{z}}' = P_x \sin\theta + P_z \cos\theta. \tag{43}$$

Similarly, we can obtain the parallel polarization on the growth plane:

TABLE I. Parameters used for the calculations.

Parameter	GaN	InN
Lattice constant[a,b] (Å)		
a	3.112	3.544
c	4.982	5.718
Piezoelectric constant[c,d] (cm/V)		
d_{15}	-1.7×10^{-10}	
d_{31}	-1.7×10^{-10}	
d_{32}	-1.7×10^{-10}	
d_{33}	3.4×10^{-10}	

[a]Reference 29.
[b]Reference 2.
[c]Reference 15.
[d]Reference 16.

$$P_x' = \mathbf{P}\cdot\hat{\mathbf{x}}' = P_x\cos\theta - P_z\sin\theta,$$
$$P_y' = \mathbf{P}\cdot\hat{\mathbf{y}}' = 0. \tag{44}$$

The strain-induced polarization P_i will lead to an electric field E_i given by

$$D_i' = \epsilon_{ij}^{p\prime} E_j' + P_i', \tag{45}$$

where D_i' is the electric displacement and $\epsilon_{ij}^{p\prime}$ is the permittivity tensor for the epilayer given by

$$\epsilon' = U\epsilon^p U^{-1} \tag{46}$$

and

$$\epsilon^p = \begin{pmatrix} \epsilon_t & 0 & 0 \\ 0 & \epsilon_t & 0 \\ 0 & 0 & \epsilon_z \end{pmatrix}, \tag{47}$$

where ϵ_t and ϵ_z are permittivities[28] perpendicular and along the c axes for the (0001) crystal orientation, respectively. Then, the electric displacement D_i' is given by

$$D_x' = (\epsilon_t\cos^2\theta + \epsilon_z\sin^2\theta)E_x' + (\epsilon_t - \epsilon_z)\sin\theta\cos\theta E_z' + P_x',$$
$$D_y' = \epsilon_t E_y' + P_y',$$
$$D_z' = (\epsilon_t - \epsilon_z)\sin\theta\cos\theta E_x' + (\epsilon_t\sin^2\theta + \epsilon_z\cos^2\theta)E_z' + P_z'. \tag{48}$$

If there are no external charges and $\epsilon_t \simeq \epsilon_z$, D_z' vanishes, and the electric field reduces to

$$E_z' \simeq -\frac{P_z'}{\epsilon_t}. \tag{49}$$

For a quantum-well structure of a width L_z, the valence-band structure is calculated by using 6×6 Hamiltonian for an arbitrary crystal orientation, which is obtained by using Eqs. (1) and (5). The piezoelectric field of the (assumed thick) barrier region can be taken as zero. The quantum-well potential due to the band-edge discontinuities of the well and barrier materials follows the model of Ref. 29 and it is added with the electrostatic potential due to the piezoelectric field to the effective mass equation, which the envelope functions $\{g_\nu^{(m)}\}$ for the mth subband satisfy as follows:

$$\sum_{\nu'}\left[H_{\nu\nu'}\left(k_x', k_y', -i\frac{\partial}{\partial z'}\right) + (V_\nu(z') + qE_z'z')\delta_{\nu\nu'}\right]g_\nu^{(m)}(k_x', k_y', z') = E_m'(k_x', k_y')g_\nu^{(m)}(k_x', k_y', z'), \tag{50}$$

where $\nu, \nu' = 1, 2, 3, 4, 5$, and 6, and E_z' is given in Eq. (49). These coupled differential equations can be solved using a finite-difference method.[29]

III. NUMERICAL RESULTS AND DISCUSSION

In this section, we present numerical results for the crystal orientation dependencies of important physical quantities such as the band gap, strain, wave functions, optical matrix elements, and piezoelectric polarization. As a numerical example, we consider the situation where a GaN epilayer is grown on an $In_xAl_{1-x}N$ barrier (substrate). The parameters used in the computations are taken from Refs. 13 and 29, except for those listed in Table I.

For our following discussions, it should be noted from Fig. 1 that the angle θ is defined as the angle between the growth direction (z' axis) and and the c axis (z axis), as shown in Fig. 1(a). Therefore, $\theta = 0°$ corresponds to growth along the c axis or (0001) orientation, and $\theta = 90°$ corresponds to growth along the $(10\bar{1}0)$ direction, which is perpendicular to the c axis. Crystal orientation dependencies of the investigated physical quantities of strained GaN bulk semiconductors are symmetric with respect to $\theta = 90°$, and will be shown only for the angles between $\theta = 0°$ and $\theta = 90°$, except for the piezoelectric field, which will be calculated for $0° \leqslant \theta \leqslant 180°$.

A. Band gap and strain tensors

First, we plot the transition energies corresponding to the conduction band (C) to heavy-hole (HH), light-hole (LH), and crystal-field split-off hole (CH) bands. Figures 2(a) and 2(b) show these interband transition energies near the band edges as a function of the crystal orientation for (a) -0.5% compressively ($GaN/In_{0.14}Al_{0.86}N$) and (b) 0.5% tensilely ($GaN/In_{0.22}Al_{0.78}N$) strained GaN crystals. The ground states for holes in the valence band are the HH and LH bands for the compressive and tensile strains, respectively. In the case of (0001) orientation ($\theta = 0°$) with the compressive strain, it is observed that the energy difference between the HH and LH bands is very small. For comparison, when a zinc-blende layer is grown along the (001) axis with compressive strain, the strain deformation potentials lift the HH band up and reduce its in-plane effective mass.[9] However, for a wurtzite layer grown along the (0001) orientation, the compressive

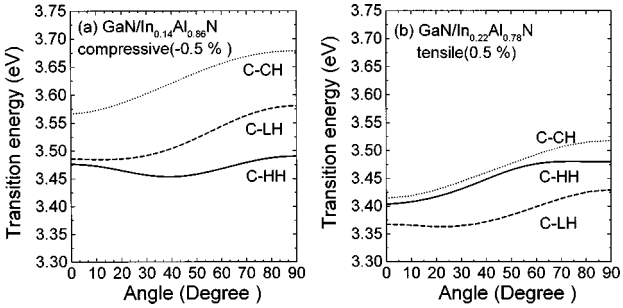

FIG. 2. Transition energies at the band edge as a function of the crystal orientation for (a) -0.5% compressively ($GaN/In_{0.14}Al_{0.86}N$), and (b) 0.5% tensilely ($GaN/In_{0.22}Al_{0.78}N$) strained GaN crystals. The angle θ is defined as the angle between the growth direction $\hat{z}'$ and the c axis, as shown in Fig. 1.

strain shifts both the HH and LH bands by almost the same amount, and the in-plane effective masses remain almost the same as those in the unstrained case.[13] Similar results are observed for GaN with a biaxial tensile strain, as shown in Fig. 2(b). However, for the compressive strain, the energy difference between the HH and LH bands increases with the angle θ between the growth direction and the c axis, and shows a maximum at the $(10\bar{1}0)$ orientation ($\theta=90°$). Thus it is expected that the in-plane effective mass is largely reduced for the $(10\bar{1}0)$ orientation. Similarly, the tensile strain shows that the energy difference between the two lowest bands (LH and HH) increases with the angle θ, until about 60°, where a further increase of the angle results in a decrease of the energy difference.

Figures 3(a) and 3(b) show the band gaps at the band edges as a function of the crystal orientation for various amounts of (a) compressive and (b) tensile strains. The band gaps for compressive and tensile strains correspond to C-HH and C-LH transitions, respectively. The band gap of the compressive strain crystals increases with the strain, while that of the tensile strain crystals decreases with the strain. The shift of the band gap as a function of strain is determined mainly by the hydrostatic energy shift of the conduction-band edge, the sign of which is positive for the compressive strain and negative for the tensile strain. The band gap as a function of orientation shows a maximum at the $(10\bar{1}0)$ orientation ($\theta=90°$) for both compressive and tensile strains.

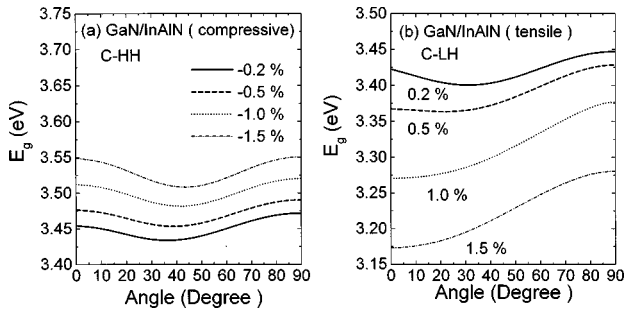

FIG. 3. Band gaps near the band edges as a function of the crystal orientation for various (a) compressively and (b) tensilely strained GaN crystals. The band gaps for compressive and tensile strains correspond to C-HH and C-LH transitions, respectively.

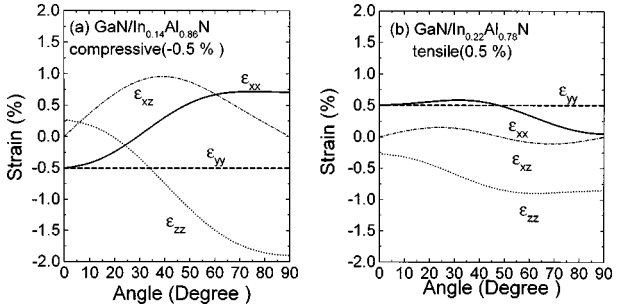

FIG. 4. Strain tensor elements as a function of crystal orientation θ for (a) -0.5% compressively ($GaN/In_{0.14}Al_{0.86}N$) and (b) 0.5% tensile ($GaN/In_{0.22}Al_{0.78}N$) strained GaN crystals.

In Figs. 4(a) and 4(b), we plot the strain tensor elements as a function of crystal orientation θ for (a) -0.5% compressively ($GaN/In_{0.14}Al_{0.86}N$) and (b) 0.5% tensilely ($GaN/In_{0.22}Al_{0.78}N$) strained GaN crystals. Note that the component ϵ_{yy} is constant and the component ϵ_{xz} is zero for the (0001) orientation ($\theta=0°$). The strain components ϵ_{xx} and ϵ_{zz} show a maximum at $\theta=90°$. Since the crystal orientation dependence of the bands is determined mainly by these strain components, the band gap shows a maximum for the $(10\bar{1}0)$ growth direction, as shown in Fig. 2. In the case of the tensile strain, it is observed that its band gap difference between the $\theta=0°$ and 90° growth directions is larger than that of the compressive strain. This is attributed to the fact that, for the tensile strain, the band gap is given by the C-LH transition and the orientation dependence of the LH band is larger than that of the HH band, as shown in Fig. 2.

B. Energy-band structures and wave functions

In addition to the band gap, the valence-band structures and the wave functions as a function of the crystal orientation show interesting features. The valence band mixing effects can be understood from the energy dispersion relations and their corresponding wave functions of the HH, LH, and CH bands. The valence-band structures and the wave functions of the bulk wurtzite GaN with the (0001) orientation has been extensively investigated.[13] However, little work has been done so far to understand the crystal orientation effects of the wave functions for the wurtzite semiconductors.

Figures 5(a)–5(c) show the calculated valence-band dispersion relations of a -0.5% compressively strained GaN crystal for (a) $\theta=0°$, (b) $\theta=45°$, and (c) $\theta=90°$. The dispersion relations are calculated numerically from the 6×6 Hamiltonian in the (x',y',z') coordinates. The full 6×6 Hamiltonian has to be used since the previous block-diagonalization methods are restricted either to the (0001) growth direction or to the zone center ($k_x'=k_y'=k_z'=0$) case [Eqs. (17)–(23)]. The band-edge effective masses can be estimated from a parabolic band fitting to the calculated dispersion relations near the band edges. The crystal orientation effects of the band-edge effective mass is useful for an understanding of optical processes such as the optical gain as well as electronic transport processes.

We know from Figs. 5(a)–5(c) that the HH band-edge effective masses along the k_y' direction are nearly constant independent of the crystal orientation. On the other hand, it

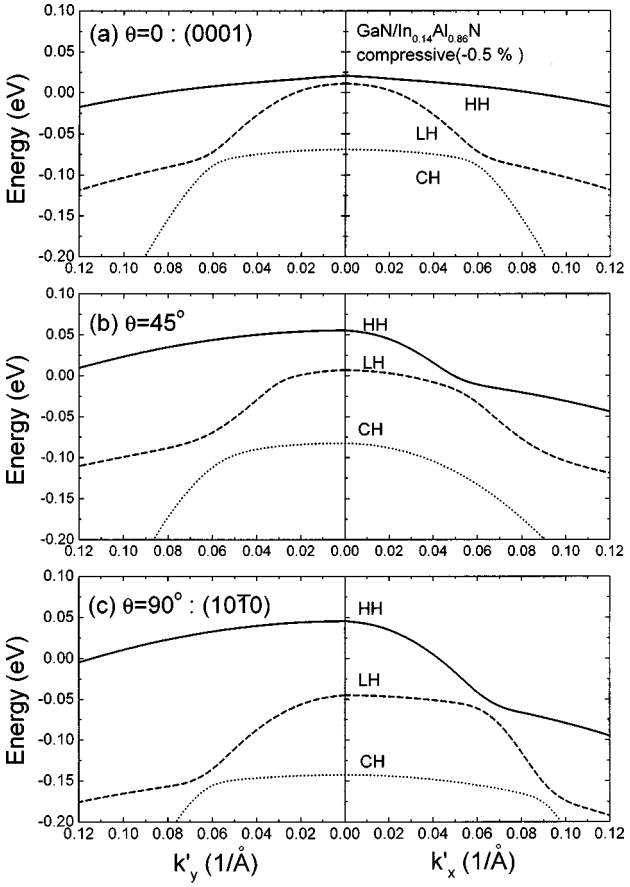

FIG. 5. Calculated valence-band dispersion relations of a -0.5% compressively strained GaN crystal for (a) $\theta=0°$, (b) $\theta=45°$, and (c) $\theta=90°$.

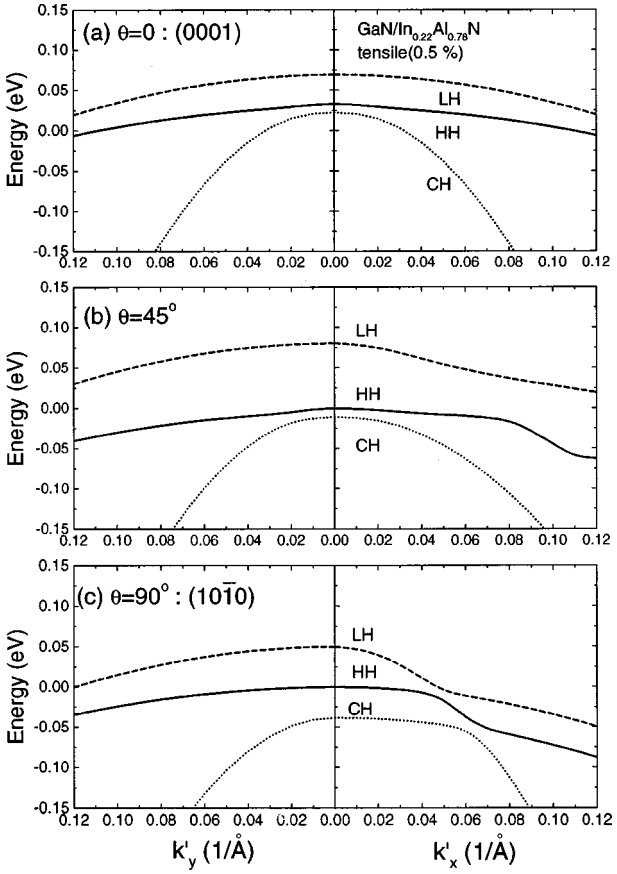

FIG. 6. Calculated valence-band dispersion relations of a 0.5% tensilely strained GaN crystal for (a) $\theta=0°$, (b) $\theta=45°$, and (c) $\theta=90°$.

is shown that the HH band-edge effective masses along the k_x' direction depend on the crystal orientation. The increase of the angle results in the reduction of the effective mass of the HH band along the k_x' direction. For example, the effective masses near the band edge are about $1.1m_0$ and $0.16m_0$ for $\theta=0°$ and 90°, respectively, along the k_x' direction. This is mainly attributed to the fact that the energy difference between the HH and LH bands increases with the angle between the growth direction and the c axis from Fig. 2. A similar situation is observed for the LH band of the tensile strain case. In Figs. 6(a)–6(c), we plot the calculated valence-band dispersion relations of a 0.5% tensilely strained GaN crystal for (a) $\theta=0°$, (b) $\theta=45°$, and (c) $\theta=90°$. For the tensile strain, the top valence band is the LH band and its effective mass along the k_x' direction is reduced with an increasing growth angle θ. Thus it is expected that the $(10\bar{1}0)$ orientation ($\theta=90°$) should improve the performance of both compressively and tensilely strained GaN-based lasers due to its reduced effective mass.

Figures 7(a)–7(c) show the normalized valence wave functions at the band edge of a -0.5% compressively strained GaN crystal for the (a) HH, (b) LH, and (c) CH bands. The vth valence-band wave function as a function of the crystal orientation is determined by the eigenfunctions of Eq. (28). The mixing ratio of the coefficients g_1', g_2', and g_3' determines the nature of each band. For the (0001) orientation ($\theta=0°$), the HH band is decoupled from the LH and CH bands. Thus we obtain $g_1'=1$ and $g_2'=g_3'=0$, as shown in Fig. 7(a), and $g_1'=0$ for the LH and CH bands, as shown in Figs. 7(b) and 7(c). The LH band is dominated by the g_2' component, with a small amount of mixing with the g_3' component. Similarly, the CH band is dominated by the g_3' component with a small amount of mixing with the g_2' component.

On the other hand, with an increasing angle θ, the HH band in Fig. 7(a) shows a rapid decrease of the g_1' component and a rapid increase of the g_3' component with a small increase of the g_2' component. Thus strong mixing between all three components is observed around $\theta=25°$, and the HH band is dominated by the g_3' component with a further increase of the angle. The g_2' and g_1' components for the LH band in Fig. 7(b) also show a behavior similar to the HH band. However, the two components are nearly constant in the range above 45°. Thus strong mixing between the g_1' and g_2' components is observed near the $(10\bar{1}0)$ orientation ($\theta=90°$), while the g_3' component is negligible. The CH band in Fig. 7(c) also shows a strong mixing between the g_1' and g_2' components near the $(10\bar{1}0)$ orientation.

Figures 8(a)–8(c) show the normalized valence wave functions at the band edges of a 0.5% tensilely strained GaN crystal for the (a) HH, (b) LH, and (c) CH bands. For the (0001) orientation ($\theta=0°$), the HH band in Fig. 8(a) is decoupled from the LH and CH bands as in the case of the

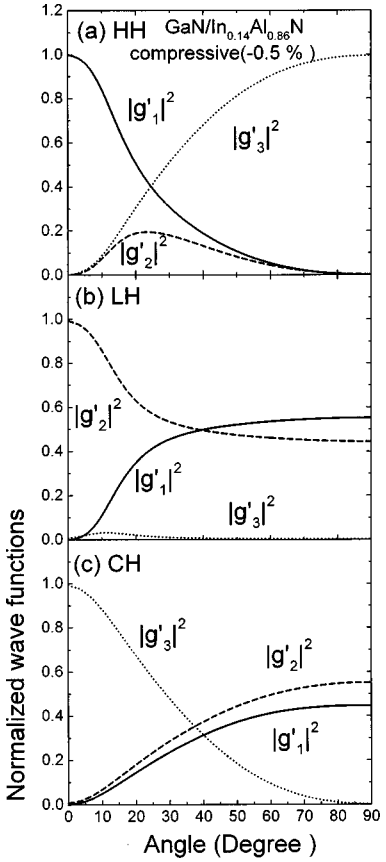

FIG. 7. Normalized valence wave functions at the band edge of a −0.5% compressively strained GaN crystal for the (a) heavy-hole (HH), (b) light-hole (LH), and (c) crystal-field split-off hole (CH) bands.

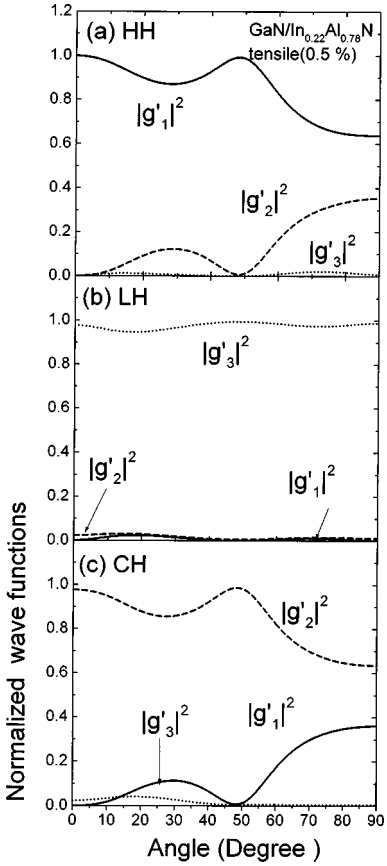

FIG. 8. Normalized valence wave functions at the band edges of 0.5% tensilely strained GaN crystal for the (a) HH, (b) LH, and (c) CH bands.

compressive strain in Fig. 7(a). The LH band in Fig. 8(b) is dominated by the g_3' component, while the CH band in Fig. 8(b) is dominated by the g_2' component. With an increasing angle, the HH and CH bands generally show a mixing between g_1' and g_2'. On the other hand, the LH band is dominated by the g_3' component, and the g_1' and g_2' components are nearly zero for all orientations. Since the optical momentum matrix elements are mainly determined by the behavior of these wave functions, it is expected that momentum matrix elements are significantly affected by the crystal orientation, as discussed below.

C. Optical momentum matrix elements

From the band-edge eigenvalues and wave functions, we calculate the optical momentum matrix elements as a function of the crystal orientation for a GaN semiconductor, which is important for the interband optical transition. Figures 9(a) and 9(b) show the interband optical momentum matrix elements at the band edges as a function of crystal orientation θ for the (a) TE and (b) TM polarizations of a −0.5% compressively strained GaN crystal. For the (0001) orientation ($\theta=0°$), the interband optical matrix elements for the HH and LH bands to the conduction band are dominated by the TE polarization, as shown in Fig. 9(a), and the interband transition between the CH band and the conduction band is dominated by the TM polarization, as shown in Fig. 9(b). With an increasing angle θ, the TE optical matrix element for the C-LH transition rapidly decreases, and is nearly zero above $\theta=30°$. On the other hand, the TE optical matrix element for the C-HH transition rapidly increases and approaches a constant value above $\theta=30°$. The constant value is about two times as large as that of the (0001) orientation. This can be explained by the crystal orientation dependence of the wave functions. As the angle increases, the HH wave function is dominated by the g_3' component, as shown in Fig. 7(a), which determines the optical matrix element for the C-HH transition. On the other hand, the LH and CH bands show a mixing of the g_1' and g_2' components. However, the g_1' and g_2' contributions to the optical matrix elements of the

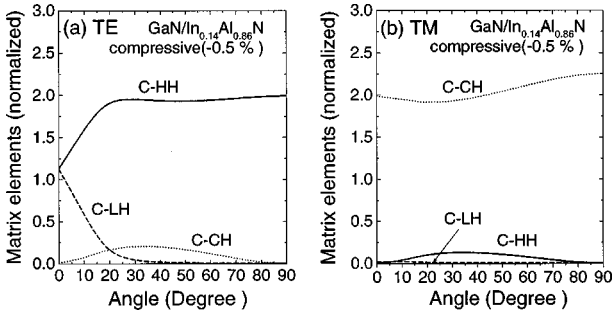

FIG. 9. Interband optical momentum matrix elements at the band edges as a function of crystal orientation for the (a) TE and (b) TM polarizations of a −0.5% compressively strained GaN crystal.

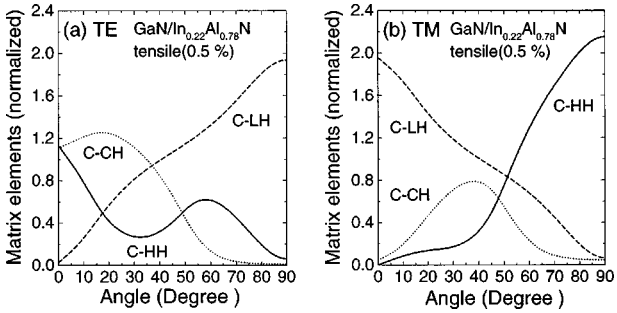

FIG. 10. Optical momentum matrix elements at the band edges as a function of crystal orientation for the (a) TE and (b) TM polarizations of a 0.5% tensile strained GaN crystal.

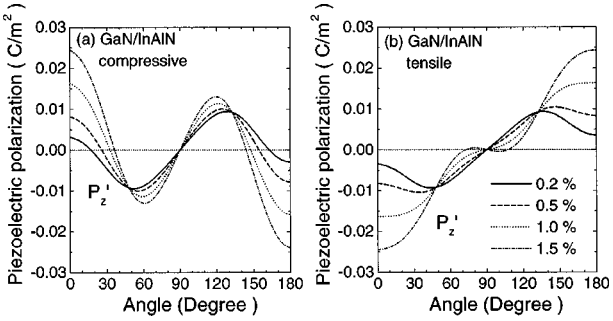

FIG. 11. Strain-induced normal polarization (P_z') with respect to the growth plane as a function of the angle θ between the growth direction and the c axis for (a) compressively and (b) tensile strained GaN crystals.

C-LH and C-CH transitions cancel each other out by an opposite sign, as shown in Eq. (34). Similarly, the contributions of the C-HH and C-LH transitions for the TM polarization cancel each other out. Thus the TM polarization matrix element is dominated by the interband transition between the CH band and the conduction band, as shown in Fig. 9(b).

Figures 10(a) and 10(b) show the optical momentum matrix elements at the band edges as a function of crystal orientation for the (a) TE and (b) TM polarizations of 0.5% tensilely strained GaN crystals. For the (0001) orientation ($\theta=0°$), the interband optical matrix elements for the C-HH and C-CH transitions are dominated by the TE polarization, and the C-LH transition is dominated by the TM polarization. On the other hand, at an angle near the $(10\bar{1}0)$ orientation ($\theta=90°$), the interband optical matrix elements for the C-LH and C-HH transitions are dominated by the TE and TM polarizations, respectively. The optical matrix elements for the C-LH transition behaves like $\cos^2\theta$ and $\sin^2\theta$ for the TE and TM polarizations, respectively, because the wave function of the LH band is dominated by the g_3' component. On the other hand, the optical matrix elements for the C-HH and C-CH transitions are mainly determined by g_1' and g_2' components. They show interesting oscillatory behavior due to the oscillatory behavior of g_1' and g_2', as shown in Fig. 8.

D. Piezoelectric field and valence-band structures of a quantum well

Wurtzite GaN, with a large piezoelectric constant and a wide band gap, has potential applications such as piezoelectric sensors and high electron mobility transistors (HEMT's).[30] On the other hand, the electrical and optical properties of GaN-based lasers can be affected by the large piezoelectric field. For example, it has been shown recently that the optical gain in QW lasers is largely reduced due to the piezoelectric field.[18,19] Thus it is important to control the magnitude and direction of the piezoelectric field depending on the requirements of the physical properties. In this section, we investigate the crystal orientation effects of the piezoelectric field.

Figures 11(a) and 11(b) show the strain-induced normal polarization (P_z') with respect to the growth plane as a function of the angle θ between the growth direction and the c axis for (a) compressively and (b) tensilely strained GaN crystals. The normal polarization P_z' is important because the GaN-based QW structures have quantized energy levels along the growth direction. The normal polarization leads to an accumulation or a depletion of carriers at the interfaces, and creates a piezoelectric field. On which side of the interfaces the accumulation region is produced depends on the type of atomic plane at the interface (Ga or N) in structures such as QW and semiconductor-insulator-semiconductor.[14] The normal polarization is asymmetric with respect to the $(10\bar{1}0)$ orientation ($\theta=90°$). The asymmetry of the normal polarization is due to the change of the atomic plane type with respect to the $(10\bar{1}0)$ orientation.

For compressively and tensilely strained GaN crystals, it is observed that the crystal orientation with the maximum normal polarization depends on the magnitude of strain. For example, GaN crystals with a larger strain show a maximum polarization for the (0001) orientation, while those with a smaller strain show the maximum polarization around ($\theta=50°$). For the (0001) orientation, the normal polarization is always positive for the compressive strain and negative for the tensile strain. However, the normal polarization for the compressive strain shows a sign change with an increasing angle, and its value depends on the strain, as shown in Fig. 11. For example, the normal polarization is negative between $\theta\simeq 17°$ and $\theta=90°$ for a compressive strain of -0.2% [solid line in Fig. 11(a)]. On the other hand, GaN with a tensile strain shows a negative normal polarization irrespective of the angle. For QW lasers, it is desirable to have no piezoelectric field because the optical gain is significantly reduced by the piezoelectric field in the well. The large piezoelectric field induces a spatial separation of the electron and hole wave functions, which results in a reduction of the transition probability between the conduction and valence subbands.[19] We know that both compressively and tensilely strained GaN crystals show zero normal polarizations for the $(10\bar{1}0)$ orientation. Thus it is expected that GaN-based lasers with a $(10\bar{1}0)$ orientation corresponding to $\theta=90°$ have better performance than those with a (0001) orientation for both compressive and tensile strain. However, the piezoelectric field may have interesting applications for HEMTs because the piezoelectric field enhances the density of the two-dimensional electron gas at the interface.[30]

Figures 12(a) and 12(b) show the strain-induced parallel polarization (P_x') as a function of the angle between the growth direction and the c axis for (a) compressively and (b)

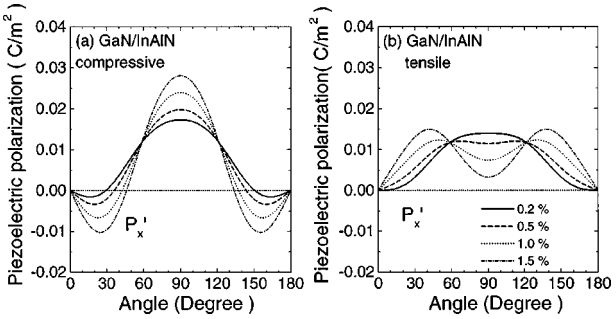

FIG. 12. Strain-induced parallel polarization (P_x') with respect to the growth plane as a function of angle between the growth direction and the c axis for (a) compressively and (b) tensile strained GaN crystals.

tensilely strained GaN crystals. It is observed that the parallel polarization (with respect to the growth plane) (P_x') is symmetric with respect to $\theta=90°$, and shows zero polarization for the (0001) orientation ($\theta=0°$) for both compressively and tensilely strained GaN crystals. For the tensile strain, the normal polarization is always positive irrespective of the angle. On the other hand, the compressive strain shows a sign change with an increasing angle similar to the normal polarization. The parallel polarization for the compressive strain case is largest for the $(10\bar{1}0)$ orientation ($\theta=90°$), while that for the tensile strain depends on the magnitude of strain. The angle with maximum polarization for the tensile strain shifts from $\theta=90°$ to a smaller angle with an increasing strain. The strain-induced polarization is purely normal for (0001) orientation, and purely parallel for the $(10\bar{1}0)$ orientation. For the general orientation, the polarization has both normal and parallel components. A parallel polarization does not generate electric fields, and does not change the QW and energy-band structures. That is, it does not directly change the QW electronic structure in the way the normal polarization does. The parallel polarization leads to birefringence for light propagating along the the growth axis.[24] These results show that electrical and optical properties of strained GaN crystals are affected significantly by the piezoelectric fields induced by the piezoelectric polarization. To investigate the piezoelectric field effects on the dispersion relations, we calculate the valence-band structure of GaN quantum-well structures.

Figure 13 shows the valence-band structure along the k_y' direction of a -0.5% compressively strained $GaN/In_xAl_{1-x}N$ quantum well with a well width of 3 nm for $\theta=0°$. The dispersion relations are calculated numerically from the 6×6 Hamiltonian in (x',y',z') coordinates with a piezoelectric field. A lifting of the Kramers degeneracy in dispersion curves due to the strain-induced piezoelectric field is observed, and its magnitude is about 3–5 meV for LH1 and HH2 subbands. These values are similar to those for GaAs-based QW structures.[25,31] Valence-band structures with a piezoelectric field show a larger energy spacing between the first two subbands (HH1 and LH1), and higher subbands (HH2 and LH2) compared to those without the piezoelectric field. The increase of the subband energy spacing reduces the carrier population in the higher subbands. However, this effect is compensated for by a decrease of the optical matrix element due to the spatial separation of the

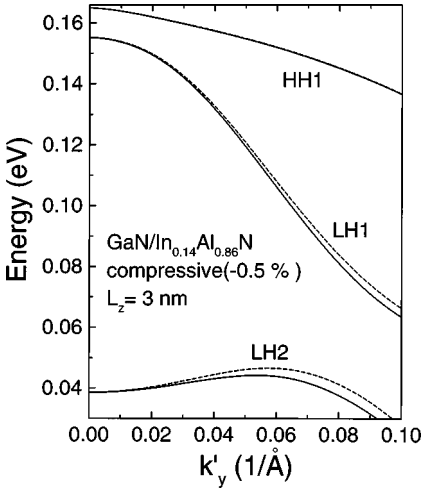

FIG. 13. The valence-band structure along the k_y' direction of a -0.5% compressively strained GaN/InAlN quantum well with a well width of 3 nm. The growth direction is along the c axis or $\theta=0°$. A lifting of the Kramers degeneracy appears in the energy splittings of the dispersion curves for a nonzero k_y'.

wave functions.[12] In Figs. 14(a)–14(c), we compare the valence-band structures of three $GaN/In_xAl_{1-x}N$ quantum-well structures of growth directions (a) $\theta=0°$, (b) $\theta=45°$, and (c) $\theta=90°$, with the same amount of strain (-0.5% compressive) and well width (3 nm). For the general orientation, the subbands are labeled by the dominant wave-

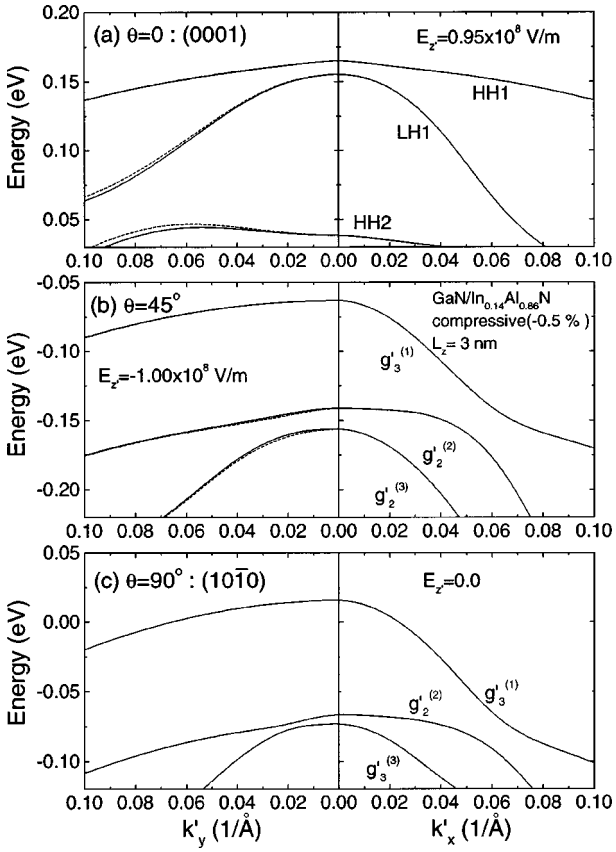

FIG. 14. Valence-band structures of three GaN/InAlN quantum-well structures with growth directions: (a) $\theta=0°$, (b) $\theta=45°$, and (c) $\theta=90°$. The amounts of strain (-0.5% compressive) and well width (3 nm) are kept the same.

function components. In a case of $\theta=90°$, there is no splitting due to zero piezoelectric field, as shown in Fig. 11. The effective masses of the first subband along the k_x' direction depend on the crystal orientation, and decrease with increasing growth angle. The reduction of the effective mass is due to the increase of the energy difference between the first two subbands. These results are in agreement with those expected from the bulk dispersion relations. The splitting in the valence-band structures is not observed along the k_x' direction, which is due to the fact that the imaginary parts of the K and H terms in Eq. (1) vanish; therefore, the upper 3×3 block become identical to the lower 3×3 block.

IV. CONCLUSIONS

We have investigated crystal orientation effects on band gaps, wave functions, and optical momentum matrix elements at the band edge of strained GaN bulk semiconductors. Also, effective masses near the band edge and the piezoelectric field have been investigated as a function of the crystal orientation. Analytical expressions for the bulk band gap, wave function, and momentum matrix element of strained wurtzite GaN using a block-diagonalized Hamiltonian have been derived. The effective mass along the k_x' direction is significantly reduced with an increasing angle θ between the growth direction and the c axis for both compressively and tensilely strained GaN crystals. The optical matrix elements of the TE polarization for the compressively strained GaN for θ above 30° is about twice as large as that of the (0001) orientation ($\theta=0°$), and is dominated by the C-HH transition. Similar results are observed in the valence-band dispersion relations for the quantum-well structure. The QW structures show a lifting of the Kramers degeneracy in their dispersion relations due to the piezoelectric field. For tensile strain, the dominant transition for the TM polarization is changed from a C-LH transition to a C-HH transition with an angle θ. It is found that a crystal orientation with a maximum piezoelectric polarization depends on the strain. In particular, the GaN crystal with a $(10\bar{1}0)$ orientation shows a zero normal polarization for the compressive and tensile strains. Thus it is expected that band-structure effects taking crystal orientation and strain into account can be used to optimize the performance of GaN-based devices such as lasers, sensors, and electroabsorption modulators. They will also determine electronic transport properties as well as optical excitation and excitonic absorption properties, such as those in photoluminescence and transmission spectra.

ACKNOWLEDGMENTS

This work was supported by ONR Grant No. N00014-96-1-0303. S.H.P. was also supported by the Catholic University of Taegu-Hyosung.

*On leave from Department of Physics, Catholic University of Taegu-Hyosung, Hayang, Kyeongbuk, Korea. Electronic address: shpark@cuth.cataegu.ac.kr

†Electronic address: s-chuang@uiuc.edu

[1] S. Nakamura, T. Mukai, and M. Senoh, Jpn. J. Appl. Phys. **30**, L1998 (1991).

[2] S. Nakamura and G. Fasol, *The Blue Green Diode* (Springer, Berlin, 1997).

[3] S. Nakamura, M. Senoh, S. Nagahama, N. Iwasa, T. Yamada, T. Matsushita, H. Kiyoku, Y. Sugimoto, T. Kozaki, H. Umemoto, M. Sano, and K. Chocho, Appl. Phys. Lett. **72**, 2014 (1998).

[4] G. L. Bir and G. E. Pikus, *Symmetry and Strain-Indeced Effects in Semiconductors* (Wiley, New York, 1974).

[5] G. E. Pikus and G. L. Bir, Fiz. Tverd. Tela (Leningrad) **1**, 1642 (1959) [Sov. Phys.—Solid State **1**, 1502 (1960)].

[6] G. E. Pikus, Zh. Eksp. Teor. Fiz. **14**, 1075 (1962) [Sov. Phys. JETP **14**, 1075 (1962)].

[7] S. L. Chuang and C. S. Chang, Appl. Phys. Lett. **68**, 1657 (1996).

[8] S. L. Chuang and C. S. Chang, Phys. Rev. B **54**, 2491 (1996).

[9] S. L. Chuang, *Physics of Optoelectronic Devices* (Wiley, New York, 1995), Chap. 4.

[10] W. Fang and S. L. Chuang, Appl. Phys. Lett. **67**, 751 (1995).

[11] M. Suzuki and T. Uenoyama, Jpn. J. Appl. Phys. **35**, L953 (1996).

[12] S. H. Park and S. L. Chuang, Appl. Phys. Lett. **72**, 287 (1998).

[13] M. Kumagai, S. L. Chuang, and H. Ando, Phys. Rev. B **57**, 15 303 (1998).

[14] A. Bykhovski, B. Gelmont, and S. Shur, Appl. Phys. Lett. **63**, 2243 (1993).

[15] A. Bykhovski, V. V. Kaminski, M. S. Shur, Q. C. Chen, and M. A. Khan, Appl. Phys. Lett. **68**, 818 (1996).

[16] G. Martin, A. Botchkarev, A. Rockett, and H. Morkoç, Appl. Phys. Lett. **68**, 2541 (1996).

[17] T. Takeuchi, S. Sota, M. Katsuragawa, H. Takeuchi, H. Amano, and I. Akasaki, Jpn. J. Appl. Phys. **36**, L382 (1997).

[18] J. Wang, J. B. Jeon, Yu. M. Sirenko, and K. W. Kim, IEEE Photonics Technol. Lett. **9**, 728 (1997).

[19] S. H. Park and S. L. Chuang, Appl. Phys. Lett. **72**, 3103 (1998).

[20] T. Ohtoshi, A. Niwa, and T. Kuroda, Jpn. J. Appl. Phys. **35**, L1566 (1996).

[21] J. M. Hinckley and J. Singh, Phys. Rev. B **42**, 3546 (1990).

[22] R. H. Henderson and E. Towe, Phys. Rev. B **78**, 2447 (1995).

[23] J. F. Nye and F. R. S., *Physical Properties of Crystals* (Clarendon, Oxford, 1989), Chaps. 5 and 6.

[24] D. L. Smith and C. Mailhiot, J. Appl. Phys. **63**, 2717 (1988).

[25] G. Bastard, *Wave Mechanics Applied to Semiconductor Heterostructures* (Halsted, New York, 1988), Chap. III.

[26] D. L. Smith and C. Mailhiot, Rev. Mod. Phys. **62**, 173 (1990).

[27] M. Abramowitz and I. A. Stegun, *Handbook of Mathematical Functions* (Dover, New York, 1972), p. 17.

[28] A. Shikanai, T. Azuhata, T. Sota, S. Chichibu, A. Kuramata, K. Horino, and S. Nakamura, J. Appl. Phys. **81**, 417 (1997).

[29] S. L. Chuang and C. S. Chang, Semicond. Sci. Technol. **12**, 252 (1997).

[30] R. Gaska, J. W. Yang, A. Osinski, A. D. Bykhovski, and M. S. Shur, Appl. Phys. Lett. **71**, 3673 (1997).

[31] D. Ahn and S. L. Chuang, J. Appl. Phys. **64**, 6143 (1988).